Action Potential and Contractility Changes in $[Na^+]_i$ Overloaded Cardiac Myocytes: A Simulation Study

Gregory M. Faber and Yoram Rudy
Cardiac Bioelectricity Research and Training Center and Department of Biomedical Engineering, Case Western Reserve University, Cleveland, Ohio 44106-7207 USA

ABSTRACT Sodium overload of cardiac cells can accompany various pathologies and induce fatal cardiac arrhythmias. We investigate effects of elevated intracellular sodium on the cardiac action potential (AP) and on intracellular calcium using the Luo–Rudy model of a mammalian ventricular myocyte. The results are: 1) During rapid pacing, AP duration (APD) shortens in two phases, a rapid phase without Na^+ accumulation and a slower phase that depends on $[Na^+]_i$. 2) The rapid APD shortening is due to incomplete deactivation (accumulation) of I_{Ks}. 3) The slow phase is due to increased repolarizing currents I_{NaK} and reverse-mode I_{NaCa}, secondary to elevated $[Na^+]_i$. 4) Na^+-overload slows the rate of AP depolarization, allowing time for greater $I_{Ca(L)}$ activation; it also enhances reverse-mode I_{NaCa}. The resulting increased Ca^{2+} influx triggers a greater $[Ca^{2+}]_i$ transient. 5) Reverse-mode I_{NaCa} alone can trigger Ca^{2+} release in a voltage and $[Na^+]_i$-dependent manner. 6) During I_{NaK} block, Na^+ and Ca^{2+} accumulate and APD shortens due to enhanced reverse-mode I_{NaCa}; contribution of $I_{K(Na)}$ to APD shortening is negligible. By slowing AP depolarization (hence velocity) and shortening APD, Na^+-overload acts to enhance inducibility of reentrant arrhythmias. Shortened APD with elevated $[Ca^{2+}]_i$ (secondary to Na^+-overload) also predisposes the myocardium to arrhythmogenic delayed afterdepolarizations.

INTRODUCTION

Ion regulation and the maintenance of ion gradients across the cell membrane are important for cell homeostasis. In cardiac tissue, ionic imbalances can be the precursor to the genesis of arrhythmias (Levi et al., 1997; Wier and Hess, 1984; Cranefield and Aronson, 1988), which may degenerate to fibrillation and sudden cardiac death. Abnormal elevations of both intracellular sodium and calcium have been observed in myocytes during conditions of metabolic compromise, including ischemia (van Echteld et al., 1991; Tani and Neely, 1990) and digitalis toxicity (Levi, 1991; Harrison et al., 1992). Intracellular sodium can also accumulate when inactivation of voltage-gated sodium channels is abnormal or incomplete, leading to a sustained inward current. This can be due to modification of inactivation by drugs (Brill and Wasserstrom, 1986), such as veratridine and aconitine, or sodium channel mutation as occurs in the LQT3-type of the long QT syndrome (Bennett et al., 1995; Dumaine et al., 1996; Chandra et al., 1998; Nagatomo et al., 1998; Clancy and Rudy, 1999). In addition, fast rates during tachycardia and fibrillation also lead to intracellular sodium accumulation. An understanding of how ionic imbalances develop and how they affect the cardiac myocyte's electrical and mechanical properties may lead to the advancement of clinical treatment or preventive strategies (Lu and de Clerck, 1993; Haigney et al., 1994; Ravens and Himmel, 1999).

The sodium–potassium pump and the sodium–calcium exchanger are two important ion-regulating transporters that play a critical role in maintaining the ionic balance across a cardiac myocyte's membrane. In addition to this function, the electrogenic nature of these transporters implies that they also have a direct effect on membrane potential. Rapid pacing and fast rates during tachyarrhythmias increase the rates of Na^+ and Ca^{2+} influx to an extent whereby sodium-potassium pump and sodium-calcium exchanger are unable to restore the ionic concentrations to normal levels. Rapid pacing has a positive inotropic effect (in healthy tissue) and the relationship between stimulation frequency and contractility has been extensively documented (Cohen et al., 1982; Wang et al., 1988). In experiments investigating cell electrophysiology, measurements of membrane potential and ion activity are attainable using microelectrodes and fluorescence techniques. However, the underlying membrane ionic currents and ion fluxes responsible for arrhythmogenic action potential changes and changes in contractility cannot be directly measured.

In this study, we use a detailed theoretical model of a cardiac myocyte (Luo and Rudy, 1994a; Zeng et al., 1995; Viswanathan et al., 1999) to investigate the effects of sodium overload on the cellular electrophysiologic behavior

Received for publication 20 September 1999 and in final form 24 January 2000.

Address reprint requests to Yoram Rudy, Director, Cardiac Bioelectricity Research and Training Center, 509 Wickenden Building, Case Western Reserve University, Cleveland, OH 44106-7207. Tel: 216-368-4051; Fax: 216-368-8672; E-mail: yxr@po.cwru.edu. *Abbreviations used:* I_{NaK}, sodium–potassium pump current; I_{NaCa}, sodium–calcium exchange current; AP, action potential; APD, action potential duration; CICR, calcium-induced calcium release; BCL, basic cycle length; $[Na^+]_i$, intracellular sodium concentration; $[Ca^{2+}]_i$, intracellular calcium concentration; $[Ca^{2+}]_{i,max}$, peak intracellular calcium concentration; V_{max}, maximum membrane potential; dV/dt_{max}, maximum rate of change of membrane potential; DAD, delayed afterdepolarization; SR, sarcoplasmic reticulum; I_{rel}, calcium release from the SR; $I_{K(Na)}$, sodium-activated potassium current; $I_{Ca(L)}$, L-type calcium current; I_{Ks}, slow component of the delayed rectifier potassium current; I_{Kr}, rapid component of the delayed rectifier potassium current.

0006-3495/00/05/2392/13 $2.00

and on the calcium transient (the trigger of contraction). The use of a comprehensive ionic-based model permits us to directly observe transmembrane currents and ion fluxes continuously during the AP. This can be done in a controlled fashion for different pacing rates and different imposed conditions of sodium elevation. Special attention is given to the roles of I_{NaCa} and I_{NaK} in ion regulation and their effects on AP morphology. In addition, the contribution of $I_{K(Na)}$ to AP shortening during sodium overload is evaluated.

METHODS

Cell model

The theoretical Luo–Rudy (LRd) model of a mammalian ventricular action potential (Luo and Rudy, 1994a; Zeng et al., 1995; Viswanathan et al., 1999) (Fig. 1) provides the basis for the simulations in this study. The model is based mostly on guinea pig experimental data; it includes membrane ionic channel currents that are formulated mathematically using the Hodgkin–Huxley approach and ionic pumps and exchangers. The model also accounts for processes that regulate intracellular concentration changes of Na^+, K^+, and Ca^{2+}. Intracellular processes represented in the model include Ca^{2+} uptake and Ca^{2+} release by the SR and Ca^{2+} buffering by calmodulin and troponin (in the myoplasm) and calsequestrin (in the SR). For the purpose of this study, the formulations of I_{NaK}, I_{NaCa}, and the CICR process are adjusted to cover the range of greatly elevated intracellular Na^+ and Ca^{2+} (Appendix). In addition, $I_{K(Na)}$ is incorporated in the model (see below).

Na^+-activated K^+ current, $I_{K(Na)}$

It has been suggested that $I_{K(Na)}$ may play a significant role in APD shortening during conditions of elevated $[Na^+]_i$ (Kameyama et al., 1984; Levi et al., 1997; Veldkamp et al., 1994). To investigate this possibility, a formulation for $I_{K(Na)}$ is incorporated into the LRd model. $I_{K(Na)}$ is modeled as an outwardly rectifying (Luk and Carmeliet, 1990) time-independent current with $[Na^+]_i$ and voltage dependence (Kameyama et al., 1984; Sanguinetti, 1990). It is highly selective (Wang et al., 1991) for K^+ and has a maximum conductance ($\bar{g}_{K(Na)}$) of 0.12848 mS/cm^2. Formulation of this current is provided in the Appendix. The current–voltage (I–V) relationship of $I_{K(Na)}$ is shown in Fig. 2. It is linear within the physiological range of membrane voltages, and the current is less than 0.05 μA/μF for concentrations of $[Na^+]_i$ smaller than 10 mM.

Simulation protocols

For all simulations, unless otherwise specified, $[K^+]_o$ = 4.5 mM, $[Na^+]_o$ = 140 mM, and $[Ca^{2+}]_o$ = 1.8 mM. The cell remains at rest until a steady state of intracellular ionic concentrations is achieved before the application of the first stimulus. For simulations that involve $[Na^+]_i$ clamp protocols (where $[Na^+]_i$ is set to a specific concentration), $[Na^+]_i$ is clamped to an assigned value just before application of the pacing stimulus. A stimulus of -80 μA/μF is applied for a duration of 0.5 ms. A discrete

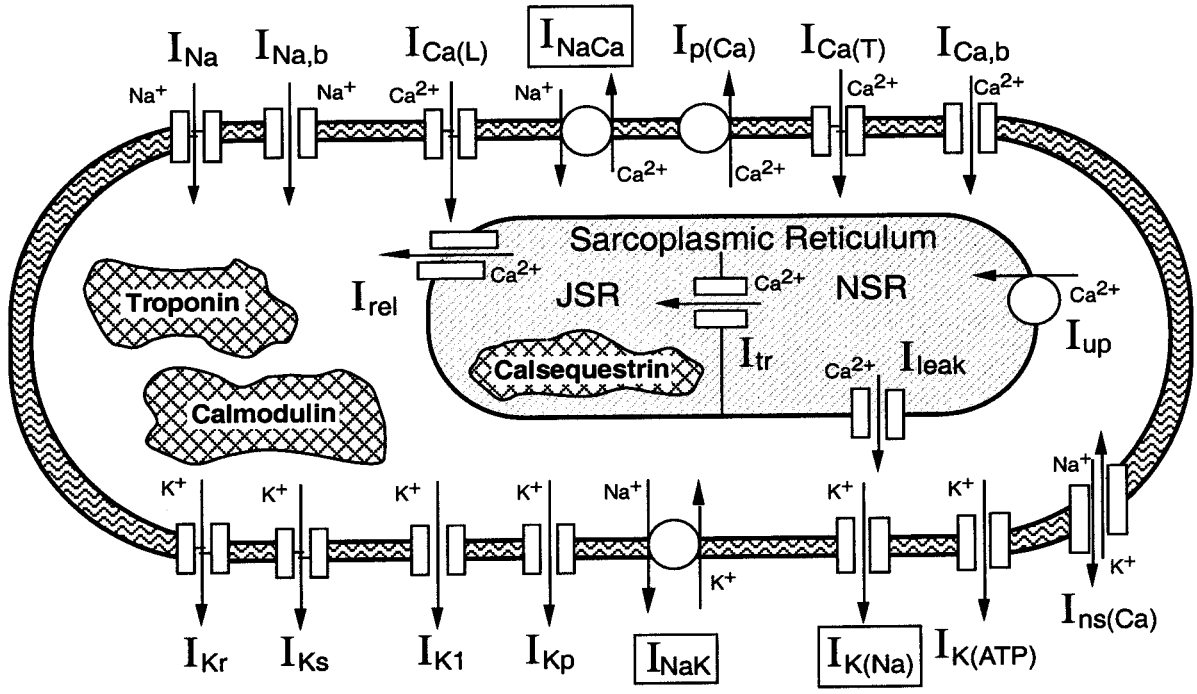

FIGURE 1 Schematic diagram of the dynamic Luo–Rudy (LRd) mammalian ventricular cell model. The major ion transporters, the sodium–potassium pump current, I_{NaK} and the sodium–calcium exchange current, I_{NaCa}, are highlighted, as well as the sodium-activated potassium current, $I_{K(Na)}$. Additional currents of significance in this study: I_{Na}, fast sodium current; $I_{Ca(L)}$, calcium current through L-type calcium channels; $I_{Ca(T)}$, calcium current through T-type calcium channels; I_{Kr}, fast component of the delayed rectifier potassium current; I_{Ks}, slow component of the delayed rectifier potassium current; $I_{p(Ca)}$, calcium pump in the sarcolemma; $I_{Ca,b}$, calcium background current; I_{up}, calcium uptake from the myoplasm to network sarcoplasmic reticulum (NSR); I_{rel}, calcium release from the junctional sarcoplasmic reticulum (JSR). For details see Luo and Rudy (1994a), Zeng et al. (1995), and Viswanathan et al. (1999). The LRd model code can be downloaded from the research sectoin of http://www.CWRU.edu/med/CBRTC.

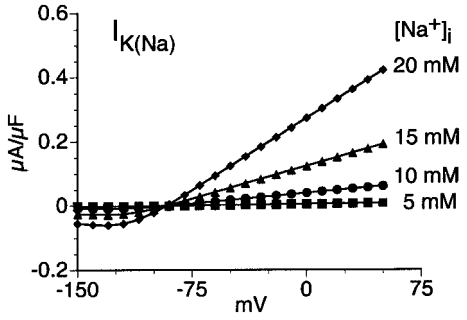

FIGURE 2 Current–voltage relationship of $I_{K(Na)}$, the Na^+-activated K^+ current. Current–voltage relationships are shown for 5 mM (■), 10 mM (●), 15 mM (▲), and 20 mM (♦) $[Na^+]_i$. All curves are obtained with 132 mM $[K^+]_i$ and 4.5 mM $[K^+]_o$.

time step of 1 ms is used in the computations except for the 20 ms after the start of the pacing stimulus, when 2 μs is used. APD is measured as the interval between the time of dV/dt_{max} and 90% repolarization (APD_{90}).

RESULTS

I_{NaCa} and I_{NaK} increase in magnitude with increasing $[Na^+]_i$

An important step in investigating the effects of elevated $[Na^+]_i$ on the electrical and contractile properties of the myocyte is to characterize its effect on processes that regulate ionic concentrations. Two important ion transporters that are affected by alterations in $[Na^+]_i$ are I_{NaCa} and I_{NaK}. Due to the electrogenic nature of these transporters, alterations of their function can have a direct affect on AP morphology. In Fig. 3, *I–V* relationships of these two transporters are shown for varying $[Na^+]_i$.

The *I–V* relationship for I_{NaCa} (Fig. 3 *A*) closely duplicates the experimental findings of Matsuoka and Hilgemann (1992). Several properties of I_{NaCa} are demonstrated, including saturation of the current with increasing voltage and increasing $[Na^+]_i$ (*inset*), and a shift of the reversal potential to more hyperpolarized potentials with increasing $[Na^+]_i$. This shift implies that I_{NaCa} operates in its reverse mode (bringing in Ca^{2+} and extruding Na^+ with 1:3 stoichiometry, generating a repolarizing current) for a longer duration during the AP, shifting the balance in favor of Ca^{2+} loading. The model simulates the experimental behavior, including the "jump" in current magnitude between 10 and 20 mM $[Na^+]_i$ (*arrow*) and the saturation at high voltage and $[Na^+]_i$.

The *I-V* relationship for I_{NaK} (Fig. 3 *B*) duplicates quite well the experimental findings of Nakao and Gadsby (1989). Of importance is the increase in current magnitude due to both an increase in voltage and an increase in $[Na^+]_i$.

Ion accumulation during pacing

During pacing, ions accumulate within the cell and intracellular ionic concentrations, specifically $[Na^+]_i$ and $[Ca^{2+}]_i$, differ greatly from those of the quiescent myocyte. The relationship between ionic concentrations and pacing

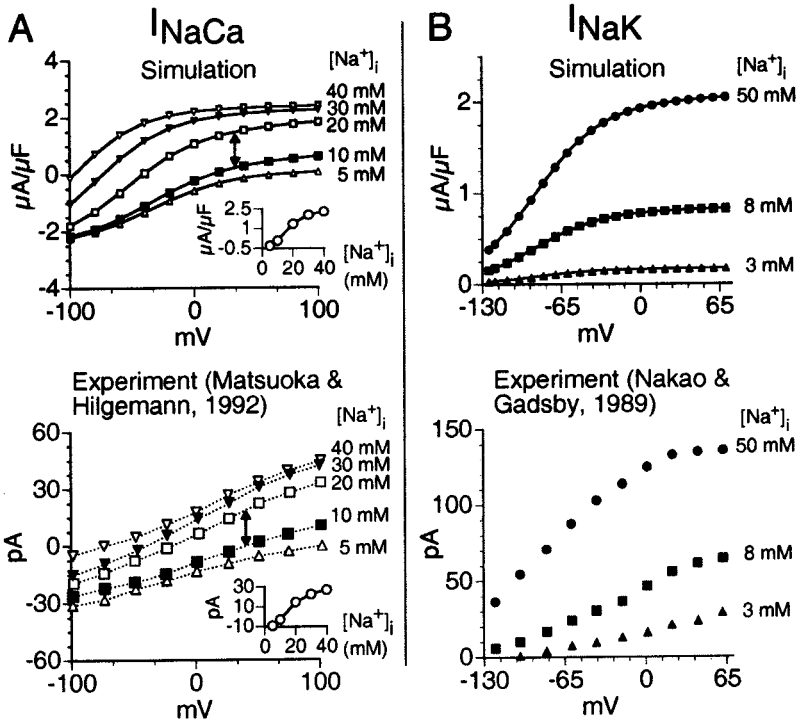

FIGURE 3 Current–voltage relationships for I_{NaCa} and I_{NaK} as a function of $[Na^+]_i$. (*A*) Simulated (*top*) and experimentally measured (*bottom*, adapted from Matsuoka and Hilgemann, 1992) I_{NaCa} *I–V* relationships for 5 mM (△), 10 mM (■), 20 mM (□), 30 mM (▼), and 40 mM (▽) $[Na^+]_i$, obtained with 1 μM $[Ca^{2+}]_i$, 2 mM $[Ca^{2+}]_o$, and 150 mM $[Na^+]_o$. The insets show I_{NaCa} magnitude versus $[Na^+]_i$, measured at 20 mV, demonstrating saturation of the current with increasing $[Na^+]_i$. (*B*) Simulated (*top*) and experimentally measured (*bottom*, adapted from Nakao and Gadsby, 1989) I_{NaK} *I–V* relationships for 3 mM (●), 8 mM (■), and 50 mM (▲) $[Na^+]_i$, obtained with 5.4 $[K^+]_o$, 140 $[K^+]_i$, and 145 mM $[Na^+]_o$.

frequency can be represented in the form of a concentration-frequency staircase. Experiments conducted by Wang et al. (1988) (Fig. 4 *B*) demonstrate that both intracellular Na_i^+-activity (a^i_{Na}, a measure of $[Na^+]_i$) and twitch force (a measure of $[Ca^{2+}]_i$) increase with increasing frequency and decrease with decreasing frequency. In Fig. 4 *A*, the theoretical simulation closely reproduces the experimental results. The panels to the right of the staircases contain simulated (*top*) and measured (*bottom*) APs at the various pacing frequencies increasing from *a* to *g*. Note that APD shortens as pacing frequency increases and ion accumulation occurs.

An adaptation curve is shown in Fig. 5, summarizing the relationship between APD and pacing frequency. Steady-state APD is approximately 185 ms for cycle lengths >2000 ms and decreases to ~65 ms at a cycle length of 100 ms. $[Na^+]_i$ and peak intracellular Ca^{2+} concentration ($[Ca^{2+}]_{i,max}$) at the corresponding cycle lengths are also plotted, showing the concomitant rise of Na^+ and Ca^{2+} as cycle length decreases. The accumulation of these intracellular ions is due to the inability of the Na^+–K^+ pump and the Na^+–Ca^{2+} exchanger to balance the rate of ion entry. The rise in these intracellular ions affects several Na^+- and Ca^{2+}-dependent currents, which results in the shortening of APD and other changes in the cells' electrophysiologic properties as investigated below.

The role of I_{Ks} and $[Na^+]_i$ in APD shortening

The accumulation of intracellular ions is not the primary cause of APD adaptation, as is demonstrated in Fig. 6, where $[Na^+]_i$ is plotted versus APD for two different cycle lengths (BCL = 300 and 1000 ms). The cells are paced from rest, and reach a steady state after approximately 5 min. The beat number gives an indication of the rate of $[Na^+]_i$ accumulation, which occurs rapidly at first and then slows as the cell approaches steady state. For both BCLs, two phases of APD shortening are observed, a rapid phase with no significant change in $[Na^+]_i$, and a much slower phase with strong $[Na^+]_i$ dependence. For a BCL of 300 ms, the rapid shortening of APD occurs within the first 5–10 beats, resulting in a change in APD from 190 to 130 ms. The cause of this rapid shortening is accumulation (incomplete deactivation and residual activation) of the slow delayed rectifier K^+ current, I_{Ks}. The first five action potentials and the corresponding I_{Ks} current are shown in the inset of Fig. 6. At this cycle length, I_{Ks} does not have sufficient time to completely

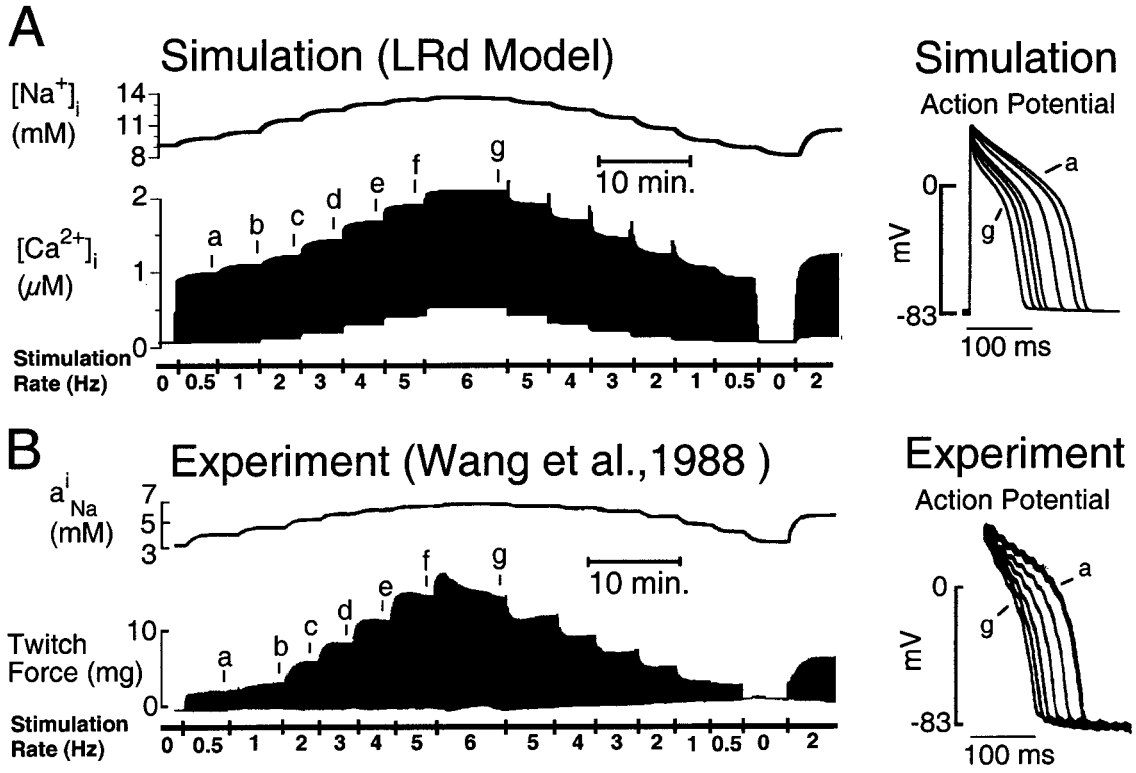

FIGURE 4 $[Na^+]_i$ and $[Ca^{2+}]_i$ as a function of pacing frequency. (*A*) Simulated concentration-frequency staircase, showing changes of $[Na^+]_i$ and $[Ca^{2+}]_i$ during a staircase protocol where frequency is stepped from 0.5 to 1 Hz and then to 6 Hz in increments of 1 Hz (5 min. at each pacing frequency). After 10 min. of pacing at 6 Hz, frequency is stepped down in reverse order. (*B*) The corresponding experiment showing measured intracellular sodium activity (a^i_{Na}) and twitch force for the same protocol (Wang et al., 1988). Both simulation and experiment were conducted using 5.4 mM $[K^+]_o$, 1.8 mM $[Ca^{2+}]_o$, and 137 mM $[Na^+]_o$. To the right of (*A*) and (*B*), the corresponding computed and measured action potentials at times a–g are shown.

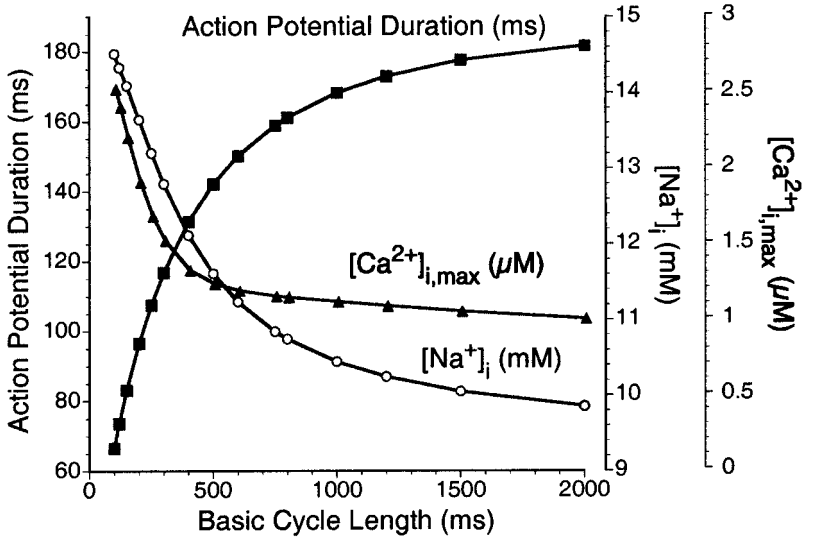

FIGURE 5 APD adaptation curve. The figure shows the steady-state relationship (achieved after 5 min. of pacing) between cycle length and APD (■) as generated by the LRd model. Corresponding changes in $[Ca^{2+}]_{i,max}$ (▲) and $[Na^+]_i$ (○) are also shown.

deactivate between beats. This results in an instantaneous jump in the current when the next stimulus is applied. The resulting greater repolarizing current acts to shorten APD. Beyond these initial beats, the magnitude of the instantaneous current does not increase, but APD continues to shorten. This is due to the gradual rise in $[Na^+]_i$. The slow accumulation of $[Na^+]_i$ alters the behavior of several Na^+-dependent currents resulting in the continued shortening. At the time when steady state is reached, $[Na^+]_i$ is responsible for ~20% of the total APD shortening, whereas I_{Ks} accumulation is responsible for ~80%. At a BCL of 1000 ms, which is more typical of human heart rate, I_{Ks} has a longer recovery time between beats, thus there is less accumulation of the current. In this case, accumulation of $[Na^+]_i$ is responsible for more than 50% of the total APD shortening. The mechanism of Na^+-dependant APD shortening is studied below.

Effects of $[Na^+]_i$ on ionic currents, action potential, and $[Ca^{2+}]_i$

To characterize the effect of elevated $[Na^+]_i$ on the AP and its underlying ionic currents, APs generated by a cell under conditions that differ only in $[Na^+]_i$ are presented in Fig. 7. The initial conditions for the two action potentials are identical (steady-state values of a quiescent cell with $[Na^+]_i$ = 10 mM) and $[Na^+]_i$ is clamped to an assigned value (10 mM or 20 mM) just before the stimulus (only one stimulus is applied). This allows examination of effects that can be attributed specifically to $[Na^+]_i$. Observed changes to the AP due to elevated $[Na^+]_i$ include reduced maximum voltage, reduced plateau potential, and shortened APD. In addition to these changes in membrane voltage, there is greater release of Ca^{2+} from the SR.

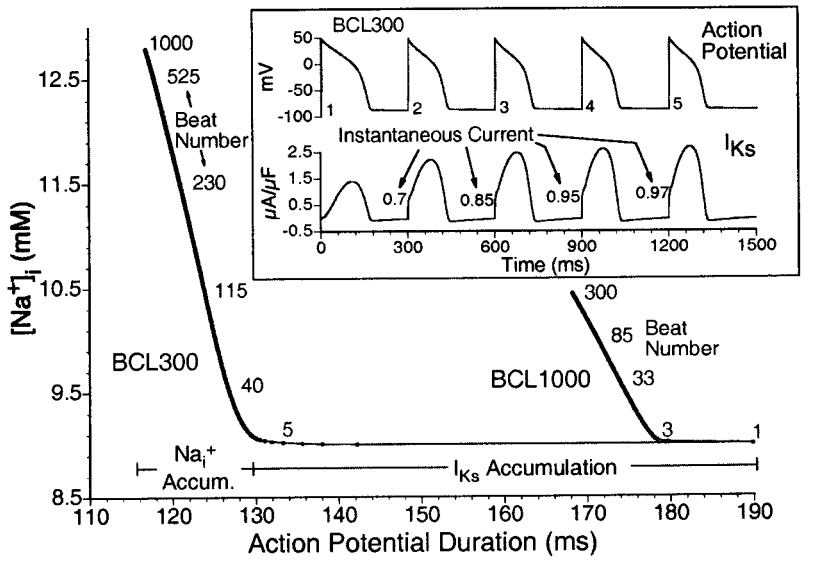

FIGURE 6 The role of $[Na^+]_i$ and I_{Ks} in APD shortening during pacing. Figure shows the relationship between $[Na^+]_i$ and APD for two different cycle lengths (BCL = 300 ms and BCL = 1000 ms). The cell is paced from rest for 5 min (1000 beats for a BCL of 300 ms and 300 beats for a BCL of 1000 ms) while simultaneous measurements of $[Na^+]_i$ and APD are made. Beat numbers are indicated to the right of each curve. For a BCL of 300 ms, the important mechanisms responsible for APD shortening are indicated beneath the curve, where I_{Ks} accumulation is responsible for approximately 80% of the total shortening and Na_i^+ accumulation is responsible for 20%. For BCL of 1000 ms, Na_i^+ accumulation is responsible for more than 50% of the total shortening. The inset shows the first five action potentials and the corresponding I_{Ks} current recorded at BCL of 300 ms. Rapid shortening of APD occurs within the first 5 beats due an increase in the instantaneous I_{Ks} current (indicated by the arrows) caused by incomplete deactivation of I_{Ks} between beats.

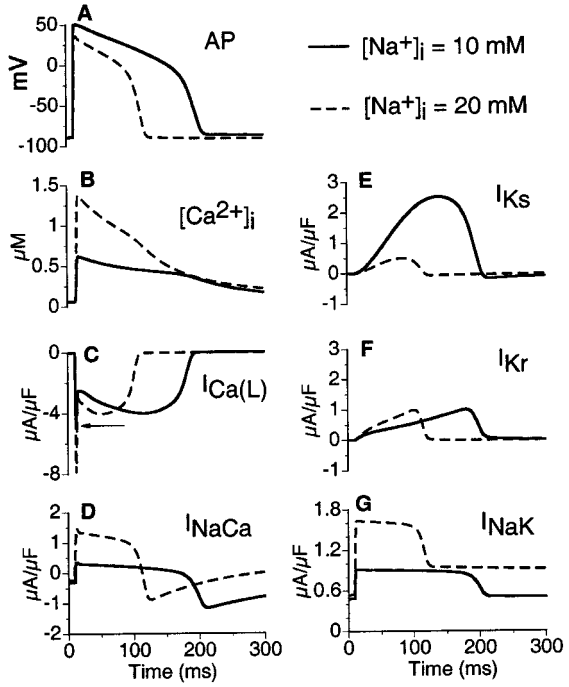

FIGURE 7 Isolated effect of elevated $[Na^+]_i$ on the action potential. The figure shows the action potential (AP), calcium transient ($[Ca^{2+}]_i$), $I_{Ca(L)}$, I_{NaCa}, I_{Ks}, I_{Kr}, and I_{NaK} for two different concentrations of intracellular Na^+, $[Na^+]_i$ = 10 mM (*solid lines*) and $[Na^+]_i$ = 20 mM (*dashed lines*). For the curve of $I_{Ca(L)}$ (*Panel C*), the arrow indicates the peak of the current for $[Na^+]_i$ = 10 mM.

The currents that are directly affected by the rise in $[Na^+]_i$ are I_{Na}, I_{NaCa}, I_{NaK}, and $I_{K(Na)}$. The role of $I_{K(Na)}$ is explored in the next section in the context of I_{NaK} block. With $[Na^+]_i$ accumulation, the reduction in the driving force decreases I_{Na}, thereby reducing the rate of AP upstroke (dV/dt_{max}) and the V_{max} (Fig. 7 *A*). Similarly, the elevated $[Na^+]_i$ drives I_{NaCa} and I_{NaK} in the outward direction (Fig. 7, *D* and *G*) providing significantly greater repolarizing current during the early stages and throughout the AP, which results in a reduced plateau potential and shortened APD (Fig. 7 *A*). Although I_{Kr} (the rapid delayed rectifier) shows no significant change (Fig. 7 *F*), the reduced AP plateau potential slows I_{Ks} activation and decreases the driving force for K^+, resulting in a greatly reduced I_{Ks} (Fig. 7 *E*). Smaller I_{Ks} is typically associated with APD prolongation, but enhanced I_{NaCa} and I_{NaK} more than compensate for this loss of repolarizing current. The "paradoxical" APD shortening with reduced I_{Ks} demonstrates the delicate balance of currents that determine the AP plateau and duration.

Elevated $[Na^+]_i$ is accompanied by a large $[Ca^{2+}]_i$ transient as a result of greater Ca^{2+} entry that triggers Ca^{2+} release from the SR through the CICR process (Fig. 7 *B*, *dashed curve*). It is important to note that the increased $[Ca^{2+}]_i$ transient is not due to larger Ca^{2+} stores within the SR because both cells in this simulation have identical initial conditions, including $[Ca^{2+}]_i$ values. Therefore, the difference in the $[Ca^{2+}]_i$ transient is secondary to the difference in $[Na^+]_i$ that is imposed (clamped) before the pacing stimulus. Two sources of Ca^{2+} entry that significantly contribute to triggering SR release are the L-type Ca^{2+} channels and reverse-mode Na^+–Ca^{2+} exchanger. As can be seen in Fig. 7, *C* and *D*, the current through these channels is significantly increased at the elevated $[Na^+]_i$ case before Ca^{2+} release. The slowed action potential upstroke due to the decreased I_{Na} increases the activation time for $I_{Ca(L)}$. Also, as a consequence of the bell-shaped *I–V* relationship of $I_{Ca(L)}$ (maximum at ~10 mV, see Fig. 10) the reduced AP voltage enhances the current. The reduced AP voltage is also further away from the Ca^{2+} reversal potential, which increases the driving force for Ca^{2+}. The combination of increased channel conductance and driving force results in an increased early phase of $I_{Ca(L)}$. During the plateau, $I_{Ca(L)}$ is of similar magnitude for the two $[Na^+]_i$ levels because the greater $[Ca^{2+}]_i$ transient at elevated $[Na^+]_i$ reduces the current through Ca^{2+}-dependant inactivation, compensating for the increase in driving force.

A summary of the $[Na^+]_i$-dependent changes in AP morphology and $[Ca^{2+}]_i$ is presented in Fig. 8. The solid curves show the isolated effects of $[Na^+]_i$ increase ($[Na^+]_i$ is clamped to an assigned value just before application of a single stimulus, all other parameters are at resting steady-state values). With increasing $[Na^+]_i$, V_{max} decreases, APD shortens, dV/dt_{max} decreases, and $[Ca^{2+}]_{i,max}$ increases. Specifically, a 100% increase in $[Na^+]_i$ from 10 to 20 mM results in a decrease of V_{max} by 22%, a shortening of APD

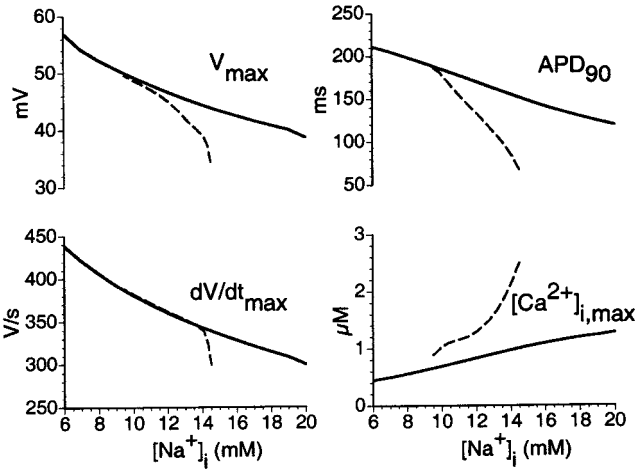

FIGURE 8 $[Na^+]_i$-dependent changes of action potential morphology and of peak $[Ca^{2+}]_i$. Changes in peak membrane voltage (V_{max}), action potential duration (APD), maximum rate of rise of the action potential upstroke (dV/dt_{max}), and peak calcium transient ($[Ca^{2+}]_{i,max}$) are shown for two different experimental protocols. The solid curves show the isolated effect of $[Na^+]_i$ changes ($[Na^+]_i$ is clamped to an assigned value just before a single stimulus; same protocol as Fig. 7). The dashed curves show values computed after 5 min. of pacing at various cycle lengths, allowing all concentrations to vary (same protocol as in Fig. 5).

by 35%, a decrease in dV/dt_{max} by 21%, and an increase in $[Ca^{2+}]_{i,max}$ by 46%.

The dashed curves in Fig. 8 are values computed using the same protocol as in Fig. 5, where the cell is paced from rest for 5 min, and all parameters and concentrations are free to change during pacing. Comparison between the paced myocyte and the $[Na^+]_i$ clamped myocyte subject to a single stimulus (*solid curves*) helps to determine the differences that occur when more than just $[Na^+]_i$ is allowed to change. Perhaps the most significant difference is the dramatic increase in $[Ca^{2+}]_{i,max}$. During pacing, $[Na^+]_i$ and $[Ca^{2+}]_i$ rise simultaneously, and the increased $[Ca^{2+}]_i$ transient is a result of both increased Ca^{2+} loading and increased triggering of release due to increased I_{NaCa} and $I_{Ca(L)}$ as discussed earlier. The more significant APD shortening observed in the paced cell is due to accumulation of I_{Ks} at faster pacing rates. Finally, the steep decrease of V_{max} and dV/dt_{max} for the paced cell is due to incomplete recovery of I_{Na} at very rapid rates.

$[Na^+]_i$-overload generated by Na^+–K^+ pump block and its ramifications

The use of Na^+–K^+ pump blockers, such as digitalis and strophanthidin, is a common treatment for relief of symptoms of heart failure (for review, see Smith et al., 1984). The mechanism by which pump blockers restore contractility begins with an elevation of $[Na^+]_i$ resulting from the loss of Na^+–K^+ pump function. This rise in $[Na^+]_i$ increases reverse-mode Na^+–Ca^{2+} exchange resulting in a rise of $[Ca^{2+}]_i$, which augments contraction and enhances cardiac function. In Fig. 9 *A*, the simulated condition of Na^+–K^+ pump block (90% reduction of I_{NaK}) is compared to experimental data from guinea pig myocytes during strophanthidin application (Levi, 1991). The simulated behavior of APD and $[Ca^{2+}]_i$ corresponds well to that observed experimentally. $[Na^+]_i$ and I_{NaCa} (not measured in the experiments) are also shown in the figure. Following the block of the Na^+–K^+ pump, $[Na^+]_i$ and $[Ca^{2+}]_i$ begin to rise. The initial brief lengthening of APD is due to the loss of the repolarizing Na^+–K^+ pump current. As $[Na^+]_i$ accumulates, reverse-mode (repolarizing) Na^+–Ca^{2+} exchange current is increased, shortening APD. The enhanced reverse-mode I_{NaCa} contributes to the rise in $[Ca^{2+}]_i$. During washout (simulated as a gradual removal of the pump block) the restored Na^+–K^+ pump current results in a period of continued APD shortening until a significant amount of $[Na^+]_i$ is removed, decreasing I_{NaCa} and I_{NaK} with a gradual prolongation of APD to its preblock value.

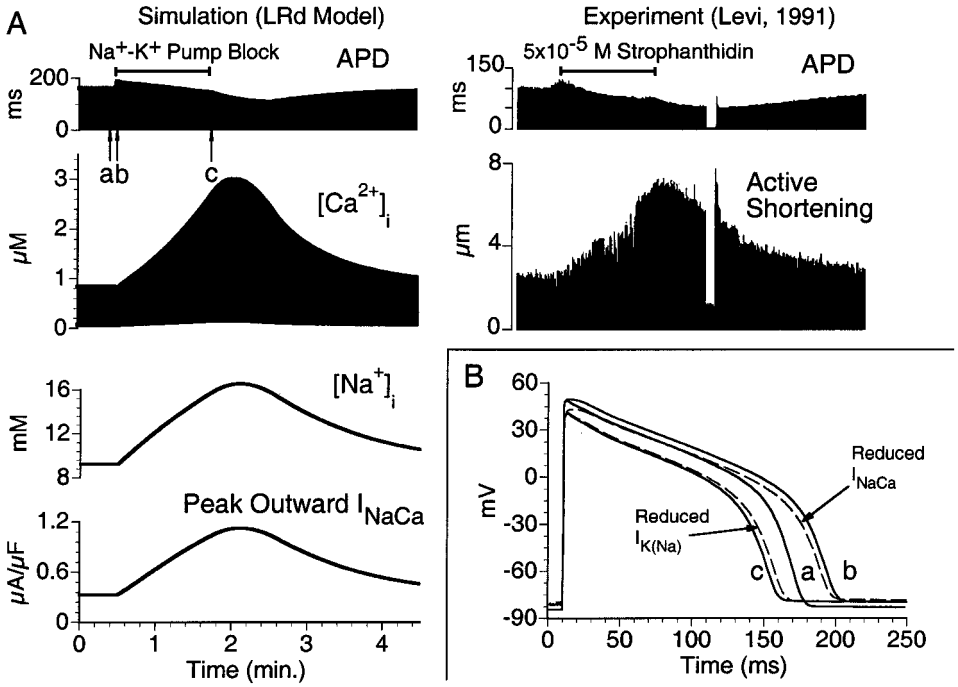

FIGURE 9 The effect of I_{NaK} block on APD; Role of I_{NaCa} and $I_{K(Na)}$ in APD shortening. (*A*) Simulated effect of I_{NaK} block on APD, $[Ca^{2+}]_i$, $[Na^+]_i$, and peak outward (reverse-mode) I_{NaCa}. On the right are corresponding experimental recordings made by Levi (1991) in a guinea pig ventricular myocyte, showing changes in APD and active shortening following the application of the I_{NaK} blocker strophanthidin (the stimulation was temporarily subthreshold, where the recorded APD is zero). For both the simulated and measured data, cells are paced at a cycle length of 1000 ms using 5.4 mM $[K^+]_o$, 1.5 mM $[Ca^{2+}]_o$, and 130 mM $[Na^+]_o$. The Na^+-activated K^+ current ($I_{K(Na)}$) is included in this simulation. (*B*) The role of I_{NaCa} and $I_{K(Na)}$ in APD shortening following I_{NaK} block. The solid curves show action potentials computed at times a, b, and c, indicated by the arrows in (*A*). The dashed curves show action potentials computed at time c, but with $I_{K(Na)}$ subjected to $[Na^+]_i$ as at time b (APD recovers by only 4 ms), or with I_{NaCa} subjected to $[Na^+]_i$ as at time b (APD recovers by approximately 35 ms, almost to the original APD at time b).

In addition to APD shortening due to an increase in reverse-mode I_{NaCa}, it has been hypothesized that the Na^+-activated K^+ current may play a significant role in APD shortening during conditions of Na^+–K^+ pump block (Kameyama et al., 1984). Its contribution is explored in Fig. 9 *B*, where APs computed at times a, b, and c of Fig. 9 *A* are shown (*solid curves*). The dashed curves are APs computed at time c ($[Na^+]_i \approx 15$ mM) with either $I_{K(Na)}$ or I_{NaCa} reduced to their values at time b ($[Na^+]_i \approx 9.2$ mM). As can be seen, I_{NaCa} accounts for almost the entire APD shortening between b and c, with minimal contribution from $I_{K(Na)}$. In Fig. 2, for $[Na^+]_i = 15$ mM and a membrane potential of 40 mV (a typical maximum voltage during an action potential), the peak $I_{K(Na)}$ current is approximately 0.15 μA/μF. Due to the linear *I–V* relationship of $I_{K(Na)}$ and its time independence, the morphology of the current during an action potential follows that of the membrane voltage. In Fig. 9, for the AP computed at time c ($[Na^+]_i \approx 15$ mM), the peak $I_{K(Na)}$ current is 0.17 μA/μF, which is less than 18% of peak I_{Kr} and less than 15% of peak I_{Ks}.

Contribution of reverse-mode I_{NaCa} to triggering SR Ca^{2+} release

The role of reverse-mode I_{NaCa} in triggering SR Ca^{2+} release is controversial, with conflicting experimental evidence for and against its ability to do so. In the previous simulations, CICR considered Ca^{2+} entry via both I_{NaCa} and $I_{Ca(L)}$ as a trigger for Ca^{2+} release from the SR. In Fig. 10, *A* and *B*, we investigate the individual roles of $I_{Ca(L)}$ and I_{NaCa} in triggering Ca^{2+} release and compare it with the release elicited when these two currents act together. In Fig. 10 *A*, where $[Na^+]_i = 10$ mM, peak $[Ca^{2+}]_i$ transient, when only $I_{Ca(L)}$ serves as a trigger (□), closely follows the bell-shaped *I–V* relationship of $I_{Ca(L)}$ (✖) as expected. A similar behavior is also observed when both $I_{Ca(L)}$ and I_{NaCa} contribute Ca^{2+} to trigger release (●). I_{NaCa} alone, in the presence of 100% $I_{Ca(L)}$ block, is able to trigger Ca^{2+} release from the SR (○). However, the resulting $[Ca^{2+}]_{i,max}$ is small compared to that elicited by $I_{Ca(L)}$ over most of the potential range shown (the relative I_{NaCa} contribution is 8% at $V = 0$ mV and 25% at $V = 40$ mV). In Fig. 10 *B*, where $[Na^+]_i = 20$ mM, $[Ca^{2+}]_{i,max}$ elicited by $I_{Ca(L)}$ alone (□) once again closely follows the $I_{Ca(L)}$ *I–V* relationship (✖). However, when $I_{Ca(L)}$ and I_{NaCa} both contribute Ca^{2+} to trigger release (●), the peak $[Ca^{2+}]_i$ transient deviates from the $I_{Ca(L)}$ *I–V* curve, especially for voltage steps to potentials greater than 20 mV. This observation, which is in agreement with results observed experimentally by several investigators (Nuss and Houser, 1992; Levi et al., 1994; Kohomoto et al., 1994; Litwin and Bridge, 1997), provides evidence for the exchanger's participation in the triggering of SR release in a voltage- and $[Na^+]_i$-dependent manner.

The results of Fig. 10 *A* cannot be readily extrapolated to the exchanger's role in triggering release during the AP at physiological $[Na^+]_i$. In Fig. 11 I, ($[Na^+]_i = 10$ mM), computed APs, and corresponding $[Ca^{2+}]_i$ transients are

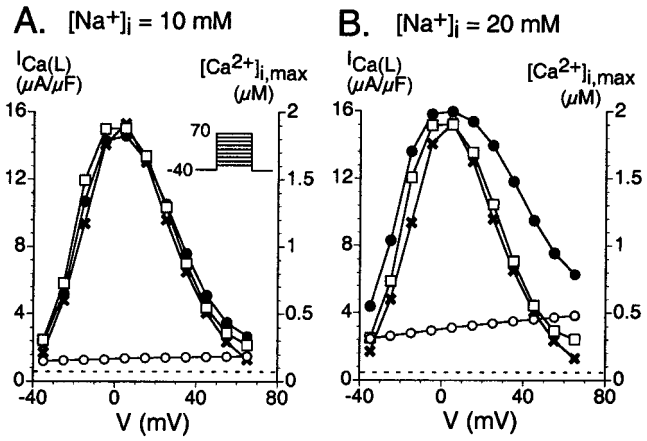

FIGURE 10 (*A* and *B*) Relationship between Ca^{2+} entry and Peak $[Ca^{2+}]_i$ for two different concentrations of $[Na^+]_i$. (*A*) ($[Na^+]_i = 10$ mM) and (*B*) ($[Na^+]_i = 20$ mM) peak $I_{Ca(L)}$ (✖; shown with reversed polarity) are shown together with three different $[Ca^{2+}]_{i,max}$ curves. These $[Ca^{2+}]_{i,max}$ curves are generated by three different modes of SR triggering: Ca^{2+} entering through any mechanism contributes to triggering SR Ca^{2+} release (●), only Ca^{2+} carried by $I_{Ca(L)}$ contributes (□), and only Ca^{2+} carried by reverse-mode I_{NaCa} contributes (○). The dashed line indicates resting $[Ca^{2+}]_i$.

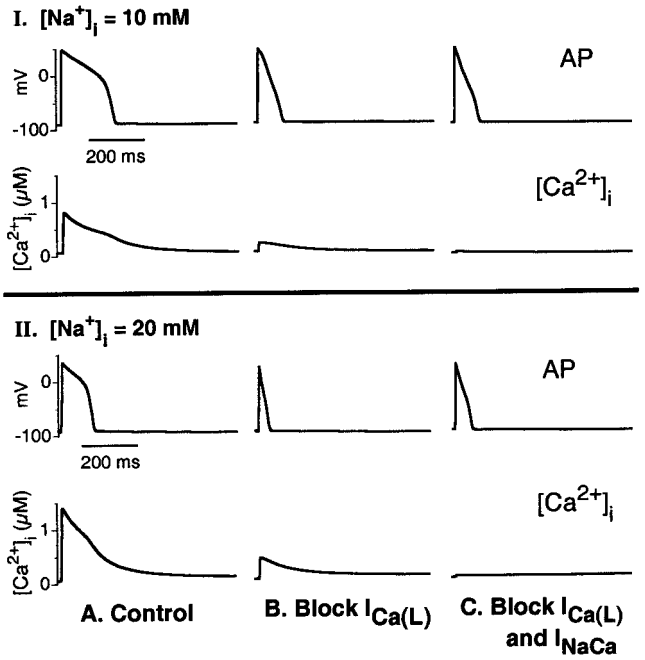

FIGURE 11 Contribution of $I_{Ca(L)}$ and I_{NaCa} to Ca^{2+} release during the action potential. Action potentials and their corresponding Ca^{2+} transients are shown for (*A*) control conditions, (*B*) conditions of $I_{Ca(L)}$ block, and (*C*) both $I_{Ca(L)}$ and I_{NaCa} block. Channel block is applied just before stimulus, ensuring equal SR loading. *Panel I* shows results for physiologic $[Na^+]_i = 10$ mM. *Panel II* shows results for elevated $[Na^+]_i = 20$ mM (sodium overload).

shown for three different protocols: (A) control, both $I_{Ca(L)}$ and I_{NaCa} contribute to signaling release; (B) $I_{Ca(L)}$ is blocked and I_{NaCa} is the primary contributor to signaling release; (C) both $I_{Ca(L)}$ and I_{NaCa} are blocked. In (B), the $[Ca^{2+}]_i$ transient elicited by I_{NaCa} triggering alone is 25% of control. In (C), there is a small residual $[Ca^{2+}]_i$ transient (only 2% of control) triggered by Ca^{2+} entry via T-type Ca^{2+} channels and background Ca^{2+} current. Note that the exchanger's contribution during the AP is consistent with its contribution during a square pulse to +40 mV (Fig. 10 *A*), a potential similar to the peak potential of the AP. Fig. 11 II shows computed APs and corresponding $[Ca^{2+}]_i$ transients for the same protocols as Fig. 11 I, but for $[Na^+]_i = 20$ mM. In this case, the $[Ca^{2+}]_i$ transient elicited by I_{NaCa} triggering alone (*panel B*) is 33% of the control.

DISCUSSION

There are several important findings of this study: 1) $[Na^+]_i$ accumulation at rapid heart rates plays an important role in APD shortening (in addition to the well-established role of I_{Ks}); the Na^+-dependent shortening is a result of increased outward I_{NaCa} and I_{NaK}. 2) APD shortening resulting from $[Na^+]_i$ overload alone (in the absence of rapid pacing) occurs despite a reduced I_{Ks} (which acts to prolong APD). 3) $I_{K(Na)}$ contributes little to APD shortening, even during conditions of elevated $[Na^+]_i$. 4) Ca^{2+} entry via both I_{NaCa} and $I_{Ca(L)}$ increases with increasing $[Na^+]_i$, triggering a larger $[Ca^{2+}]_i$ transient; at higher $[Na^+]_i$, reverse-mode I_{NaCa} alone can trigger Ca^{2+} release from the SR. 5) During I_{NaK} block, both intracellular Na^+ and Ca^{2+} accumulate, and APD shortens due to enhanced outward I_{NaCa}.

Elevated $[Na^+]_i$ plays an important role in APD shortening

It is common knowledge that rapid pacing results in shortening of APD. The ability of the myocyte to adapt its APD in response to changes in pacing frequency is primarily due to accumulation of the I_{Ks} resulting from incomplete deactivation between beats. However, we have shown that accumulation of intracellular sodium also plays an important role. The time course of these two processes is quite different. APD shortening due to I_{Ks} accumulation occurs within a few beats, whereas APD shortening due to accumulation of $[Na^+]_i$ occurs over a period of minutes. $[Na^+]_i$ accumulates due to the inability of the Na^+–K^+ pump to remove Na_i^+ at a rate that is sufficient to compensate for the increased Na^+ entry during fast pacing.

An increase in $[Na^+]_i$ results in an increase of I_{NaK} and reverse-mode I_{NaCa} (Fig. 3), both of which are repolarizing currents. Their influence on membrane potential becomes substantial under these conditions, resulting in a shortening of APD. For the protocol shown in Fig. 7, I_{NaK} and reverse I_{NaCa} account for approximately 28% of the total repolarizing current when $[Na^+]_i = 10$ mM and for 52% when $[Na^+]_i = 20$ mM. Note that both currents are of large outward magnitude at the initial phase of the AP. This acts to reduce the AP and plateau potential, which, in turn, accelerates repolarization.

$I_{K(Na)}$ contribution to APD shortening is negligible

The simulations show that $I_{K(Na)}$ is activated during sodium overload (e.g., due to compromised I_{NaK}) and acts to shorten APD. However, its quantitative effect on APD is minimal even when $[Na^+]_i$ is greatly elevated to 16 mM. The physiological function of $I_{K(Na)}$ remains unclear. One possibility is that the channel plays an important role in other cell types or species, but is a vestigial channel in the guinea pig ventricular myocyte. Another possibility is that $[Na^+]_i$ can reach values much higher than commonly believed. Using atomic absorption spectroscopy, Radford et al. (1998) measured $[Na^+]_i$ greater than 30 mM in guinea pig myocytes. These concentrations are supported by Na^+-sensitive microelectrodes recordings (Ellis, 1977), but only if an activity coefficient of 0.2 is used for converting a^i_{Na} to $[Na^+]_i$ rather than the commonly accepted value of 0.75. Based on our simulations, for concentrations of intracellular Na^+ greater than 30 mM, $I_{K(Na)}$ is significantly activated and generates a current similar in magnitude to I_{Kr} or I_{Ks}. Although whole cell concentrations of this magnitude seem unlikely, it is possible that such concentrations are achieved in a restricted subsarcolemmal space, as has been suggested by several studies (for review, see Carmeliet, 1992). Using electron probe microanalysis, Wendt-Gallitelli et al. (1993) measured a large rise in subsarcolemmal sodium ($[Na^+]_{subsarcolemmal} = 40 \pm 7$ mM) following a rapid pacing protocol, and were able to observe the opening of Na^+-activated K^+ channels in these areas of high Na^+. Important information about subsarcolemmal spaces must be obtained before a better understanding of the function of ion-regulated transporters and channels, including $I_{K(Na)}$, can be achieved. Such information includes the location and distribution of membrane ion channels relative to the subsarcolemmal spaces, the surface area of membrane exposed to these spaces, subsarcolemmal volumes, ion concentrations in these volumes, and ion diffusion rates from these restricted spaces to the bulk myoplasm.

Ca^{2+}-entry through I_{NaCa} and its role in CICR

The Na^+–Ca^{2+} exchanger plays a critical role in the Ca^{2+}-handling processes of the cell. It helps to maintain low levels of resting $[Ca^{2+}]_i$ and keeps a steady-state balance of $[Ca^{2+}]_i$ by removing Ca^{2+} that entered the myocyte through voltage-gated Ca^{2+} channels during the course of the AP. A more debated contribution of the Na^+–Ca^{2+} exchanger to

Ca^{2+} cycling is its role in the CICR process. $I_{Ca(L)}$ provides the primary source of Ca^{2+}, which signals the opening of ryanodine receptors on the SR membrane. Once opened, the SR releases its Ca^{2+} store, resulting in a 10-fold increase in $[Ca^{2+}]_i$ from 0.1 to 1 μM, which triggers contraction. The exchanger's ability to contribute to the signaling of SR Ca^{2+} release was first suggested and shown in the late 1980s (Berlin et al., 1987; Bers et al., 1988; Leblanc and Hume, 1990) and has since been extensively investigated.

Membrane structure plays in important role in the excitation–contraction process. Using immunofluorescence localization, Gao et al. (1997) have shown that L-type channel proteins are present with greatest density in the t-tubules in close proximity to SR release sites, reaffirming their important role in excitation–contraction coupling. This technique has also provided evidence for the importance of the Na^+–Ca^{2+} exchanger in CICR. Immunofluorescence of the Na^+–Ca^{2+} exchange protein (Frank et al., 1992; Kieval et al., 1992) has shown that these proteins are also present with greatest density within the t-tubules. It is possible that their localization to the t-tubules is not because of a functional role in CICR, but for efficient removal of Ca^{2+} from the high-concentration restricted space. Even so, several investigators have provided evidence suggesting that I_{NaCa} plays an important role in triggering Ca^{2+} release from the SR during CICR.

Perhaps the most persuasive evidence is experiments showing deviation of cell contraction from the $I_{Ca(L)}$ I–V relationship (Levi et al., 1994; Kohomoto et al., 1994; Litwin et al., 1996). As shown in Fig. 10, the $I_{Ca(L)}$ I–V relationship is bell-shaped with maximum current around 10 mV. For the case of elevated $[Na^+]_i$ (Fig. 10 *B*, $[Na^+]_i = 20$ mM), the $[Ca^{2+}]_{i,max}$, ● deviates significantly from this relationship for voltages >20 mV. This is due to increased Ca^{2+} entry via reverse-mode I_{NaCa}, which participates in CICR to trigger greater SR release. For normal physiological $[Na^+]_i$ of 10 mM (Fig. 10 *A*), the $[Ca^{2+}]_{i,max}$ curve follows closely the $I_{Ca(L)}$ curve, but deviates from it starting at $V = 40$ mV, indicating a contribution from I_{NaCa} for $V >$ 40 mV. Because the peak AP is in this voltage range, one expects a contribution from I_{NaCa} to triggering release during an AP for normal $[Na^+]_i$. This hypothesis is confirmed by the simulation in Fig. 11 I, where I_{NaCa} alone triggers a Ca^{2+} transient with magnitude 25% of control. As expected, the role of I_{NaCa} increases as $[Na^+]_i$ increases, contributing 33% to triggering release at $[Na^+]_i = 20$ mM (Fig. 11 II). The results of these simulations are consistent with experiments that demonstrate an attenuated contraction when $I_{Ca(L)}$ is blocked and absence of contraction when both $I_{Ca(L)}$ and I_{NaCa} are blocked (Levi, 1993; Levesque et al., 1994).

Recent experiments at physiological $[Na^+]_i$ (Vornanen et al., 1994; Litwin et al., 1998; Wasserstrom and Vites, 1999) demonstrated greater deviation of cell shortening (or tension) from the bell-shaped $I_{Ca(L)}$ curve than the simulation in Fig. 10 *A*. These quantitative differences might reflect differences in details of the protocols. They could also be due to voltage-activated Ca^{2+} release (Ferrier and Howlett, 1995), a suggested mechanism that is not included in the LRd model and requires further experimental study and characterization.

One of the interesting mechanistic findings of this study is that the initial spike of $I_{Ca(L)}$ increases with increasing $[Na^+]_i$ (Fig. 7 *C*). It is this early entry of Ca^{2+} that signals the release of Ca^{2+} from the SR. Therefore, augmentation of early $I_{Ca(L)}$ is an important contributor to the increased $[Ca^{2+}]_i$ transients observed with increased $[Na^+]_i$. The cause for the increase in early $I_{Ca(L)}$ is longer activation time of the current resulting from the slowed rising phase of the AP upstroke. In addition, the $I_{Ca(L)}$ driving force is also increased because of reduced membrane potential. As can be seen in Fig. 10, where the membrane potential is held constant using the voltage clamp protocol, there is no increase in $I_{Ca(L)}$ due to increased $[Na^+]_i$ per se.

Possible arrhythmogenic consequences of sodium overload

Sodium overload can arise as a result of a multitude of disorders. Examples include conditions of metabolic compromise, digitalis toxicity, increased Na^+ entry via the Na^+–H^+ exchange as a result of intracellular acidosis, increased Na^+ entry due to persistent I_{Na} in the long QT syndrome, LQT3, and rapid rates during episodes of tachycardia and fibrillation.

Many of the AP changes observed in our simulations can facilitate the induction and subsistence of reentrant arrhythmias. For reentry to persist, the pathlength must be greater than the wavelength (the product of APD and velocity of propagation). If this condition is not maintained, the activation front will propagate into refractory tissue and the activity will terminate. Elevated $[Na^+]_i$ reduces the transmembrane Na^+ gradient, resulting in decreased dV/dt (Fig. 8) and, thus, slowed conduction. Elevated $[Na^+]_i$ also acts to reduce APD, primarily due to increased reverse-mode I_{NaCa} and I_{NaK}. These two conditions of Na^+ overload favor stabilization of reentry through reduction of the wavelength.

Another consequence of elevated $[Na^+]_i$ is an accompanying elevation of $[Ca^{2+}]_i$. If Ca^{2+} stores within the SR become greatly overloaded, episodes of spontaneous release will occur (Wier and Hess, 1984; Luo and Rudy, 1994b). This release can activate I_{NaCa} to depolarize the cell and trigger arrhythmogenic DADs (Zeng and Rudy, 1995; Luo and Rudy, 1994b). Because DADs depolarize from rest potential, the combination of short APD and elevated intracellular Ca^{2+} that exists during Na^+ overload provides highly favorable conditions for DAD development. The DADs can provide the trigger (premature beat) for reentry to a substrate that is highly susceptible to reentrant rhythms as discussed above. It has been demonstrated that drugs that inhibit $[Na^+]_i$ and $[Ca^{2+}]_i$ overload are effective in the

prevention of arrhythmias (for review, see Ravens and Himmel, 1999).

Sodium overload may also result in a lowering of intracellular pH (acidosis) by reducing the rate of H^+ removal via the Na^+–H^+ exchange. Intracellular acidosis has been shown to result in a reduction of the magnitude of the L-type calcium current (Irisawa and Sato, 1986; Shaw and Rudy, 1997) which would lead to APD shortening. Interestingly, acidosis can also be a cause of Na^+ overload, especially following reperfusion of ischemic tissue. This suggests a potential antiarrhythmic role for Na^+–H^+ exchange blockers (for review, see Karmazyn, 1996).

Limitations of the study

The simulations are conducted using measured global intracellular values of $[Na^+]_i$ and $[Ca^{2+}]_i$ and accurately reproduce the experimentally observed behavior of the $[Ca^{2+}]_i$ transient in response to pacing and $[Na^+]_i$ loading. Several studies have provided evidence for the existence of subcellular spaces, which may have much higher concentrations of ions. The data necessary to accurately model restricted spaces are either limited or unavailable, making such an endeavor premature. With the development of higher-resolution measurement techniques for imaging structure and measuring local ionic concentrations, realistic modeling of the intracellular organization and its effects on function will become an achievable, important, and exciting goal.

Related to the above limitation is the method one uses to calculate I_{rel} (see Appendix). In the model, I_{rel} is formulated such that any source of Ca^{2+} entry is equally capable of triggering SR release. The close proximity of dihydropyridine receptors and ryanodine receptors suggests that $I_{Ca(L)}$ is the dominant pathway of Ca^{2+} entry responsible for triggering I_{rel} (Carl et al., 1995). It has been suggested that other pathways of Ca^{2+} entry (e.g., I_{NaCa}) are much less efficient in triggering release (Sipido et al., 1997). This may be due to a long diffusion time of Ca^{2+} from the sites of entry to SR release sites or due to Ca^{2+} influx that is much smaller than that through the L-type Ca^{2+} channels. In our simulations, Ca^{2+} entry via $I_{Ca(L)}$ is the major source of Ca^{2+} that triggers SR release, even under conditions of greatly elevated $[Na^+]_i$. However, under such conditions I_{NaCa} contributes to CICR and can trigger release in the absence of $I_{Ca(L)}$. In the model, the lower efficiency of I_{NaCa}, compared to $I_{Ca(L)}$ in triggering SR release, is a consequence of the smaller Ca^{2+} flux through I_{NaCa}, not of the spatial organization of the cell.

APPENDIX

Modeling $[Na^+]_i$-overload conditions with the LRd model (Viswanathan et al., 1999; Zeng et al., 1995; Luo and Rudy, 1994a): formulation of I_{rel}, I_{NaCa}, and $I_{K(Na)}$.

Ca^{2+} release from Junctional Sarcoplasmic Reticulum to myoplasm, I_{rel}

$$
\begin{aligned}
I_{rel} &= g_{rel} \cdot RyR_{open} \cdot RyR_{close} \cdot ([Ca^{2+}]_{JSR} - [Ca^{2+}]_i) \\
g_{rel} &= 150/(1+\exp\{[(I_{Ca(L)} + I_{Ca,b} + I_{p(Ca)} \\
&\qquad + I_{Ca(T)} - 2 \cdot I_{NaCa}) + 5]/0.9\}) \\
RyR_{open} &= 1/(1 + \exp((-t + 4)/0.5)) \\
&\qquad \text{rate of opening of release channels} \\
RyR_{close} &= 1 - (1/[1 + \exp((-t + 4)/0.5)]) \\
&\qquad \text{rate of closing of release channels}
\end{aligned}
$$

The value for t is set to 0 at the time of dV/dt_{max}.

Na^+–Ca^{2+} exchanger, I_{NaCa} (based on Varghese and Sell, 1997)

$$
I_{NaCa} = c_1 \cdot e^{(\gamma-1)VF/RT} \cdot \frac{e^{VF/RT} \cdot [Na^+]_i^3 \cdot [Ca^{2+}]_o - [Na^+]_o^3 \cdot [Ca^{2+}]_i}{1 + c_2 \cdot e^{(\gamma-1)VF/RT} \cdot \left(e^{VF/RT} \cdot [Na^+]_i^3 \cdot [Ca^{2+}]_o + [Na^+]_o^3 \cdot [Ca^{2+}]_i\right)},
$$

$$
c_1 = 0.00025, \quad c_2 = 0.0001, \quad \gamma = 0.15
$$

Na^+-activated K^+ current, $I_{K(Na)}$

$$
\begin{aligned}
I_{K(Na)} &= \bar{g}_{K(Na)} \cdot P_{oNai} \cdot P_{oV} \cdot (E_m - E_K), \\
\bar{g}_{K(Na)} &= 0.12848 \text{ mS/cm}^2 \\
&\qquad \text{maximum membrane conductance of } I_{K(Na)} \\
P_{oV} &= 0.8 - \frac{0.65}{(1 + \exp[(V + 125)/15])} \\
&\qquad \text{voltage dependence (Sanguinetti, 1990)} \\
P_{oNai} &= \frac{0.85}{1 + (K_D/[Na^+]_i)^n} \\
&\qquad [Na^+]_i \text{ dependence (Kameyama et al., 1984)} \\
K_D &= 66 \text{ mM}, \quad n = 2.8
\end{aligned}
$$

Other parameter values

$$
\begin{aligned}
\bar{I}_{up} &= 0.00875 \text{ mM/ms} \quad \text{maximum current through } I_{up} \\
\bar{I}_{NaK} &= 2.25\ \mu\text{A}/\mu\text{F} \quad \text{maximum current through } I_{NaK}
\end{aligned}
$$

This study was supported by grants R01-HL49054 and R37-HL33343 (to YR) from the National Heart, Lung, and Blood Institute of the National Institutes of Health, and by a Whitaker Foundation Development Award.

REFERENCES

Bennett, P., K. Yazawa, N. Makita, and A. J. George. 1995. Molecular mechanism for an inherited cardiac arrhythmia. *Nature.* 376:683–685.

Berlin, J., M. Cannell, and W. Lederer. 1987. Regulation of twitch tension in sheep cardiac Purkinje fibers during calcium overload. *Am. J. Physiol. Heart Circ. Physiol.* 253:H1540–H1547.

Bers, D., D. Christensen, and T. Nguyen. 1988. Can Ca^{2+} entry via Na^+–Ca^{2+} exchange directly activate cardiac muscle contraction? *J. Mol. Cell. Cardiol.* 20:405–414.

Brill, D. M., and J. A. Wasserstrom. 1986. Intracellular sodium and the positive inotropic effect of veratridine and cardiac glycoside in sheep Purkinje fibers. *Circ. Res.* 58:109–119.

Carl, S., K. Felix, A. Caswell, N. Brandt, W. J. Ball, P. Vaghy, G. Meissner, and D. Ferguson. 1995. Immunolocalization of sarcolemmal dihydropyridine receptor and sarcoplasmic reticular triadin and ryanodine receptor in rabbit ventricle and atrium. *J. Cell Biol.* 129:672–682.

Carmeliet, E. 1992. A fuzzy subsarcolemmal space for intracellular Na^+ in cardiac cells? *Cardiovasc. Res.* 26:433–442.

Chandra, R., C. F. Starmer, and A. O. Grant. 1998. Multiple effects of the KPQ deletion on gating of human cardiac Na^+ channels expressed in mammalian cells. *Am. J. Physiol. Heart Circ. Physiol.* 274: H1643–H1654.

Clancy, C. E., and Y. Rudy. 1999. Linking a genetic defect to its cellular phenotype in a cardiac arrhythmia. *Nature.* 400:566–569.

Cohen, C. J., H. A. Fozzard, and S. S. Sheu. 1982. Increase in intracellular sodium ion activity during stimulation in mammalian cardiac muscle. *Circ. Res.* 50:651–662.

Cranefield, F. P., and R. S. Aronson. 1988. Cardiac Arrhythmias: The Role of Triggered Activity and Other Mechanisms. Futura Publishing Company, Inc., New York.

Dumaine, R., Q. Wang, M. Keating, H. Hartmann, P. Schwartz, A. Brown, and G. Kirsch. 1996. Multiple mechanisms of Na+ channel-linked long-QT syndrome. *Circ. Res.* 78:916–924.

Ellis, D. 1977. The effects of external cations and ouabain on the intracellular sodium activity of sheep heart Purkinje fibres. *J. Physiol.* 273: 211–240.

Ferrier, G. R. and S. E. Howlett. 1995. Contractions in guinea-pig ventricular myocytes triggered by a calcium-release mechanism separate from Na^+ and L-currents. *J. Physiol.* 484:107–122.

Frank, J., G. Mottino, D. Reid, R. Molday, and K. Philipson. 1992. Distribution of the Na^+–Ca^{2+} exchange protein in mammalian cardiac myocytes: an immunofluorescence and immunocolloidal gold-labeling study. *J. Cell Biol.* 117:337–345.

Gao, T., T. Puri, B. Gerhardstein, A. Chien, R. Green, and M. Hosey. 1997. Identification and subcellular localization of the subunits of L-type calcium channels and adenylyl cyclase in cardiac myocytes. *J. Biol. Chem.* 272:19401–19407.

Haigney, M., E. Lakatta, M. Stern, and H. Silverman. 1994. Sodium channel blockade reduces hypoxic sodium loading and sodium-dependent calcium loading. *Circulation.* 90:391–399.

Harrison, S. M., E. McCall, and M. R. Boyett. 1992. The relationship between contraction and intracellular sodium in rat and guinea-pig ventricular myocytes. *J. Physiol.* 449:517–550.

Irisawa, H., and R. Sato. 1986. Intra- and extracellular actions of proton on the calcium current of isolated guinea pig ventricular cells. *Circ. Res.* 59:348–355.

Kameyama, M., M. Kakei, R. Sato, T. Shibasaki, H. Matsuda, and H. Irisawa. 1984. Intracellular Na^+ activates a K^+ channel in mammalian cardiac cells. *Nature.* 309:354–356.

Karmazyn, M. 1996. The sodium–hydrogen exchange system in the heart: its role in ischemic and reperfusion injury and therapeutic implications. *Can. J. Cardiol.* 12:1074–1082.

Kieval, R., R. Bloch, G. Lindenmayer, A. Ambesi, and W. Lederer. 1992. Immunofluorescence localization of the Na–Ca exchanger in heart cells. *Am. J. Physiol. Cell Physiol.* 263:C545–C550.

Kohomoto, O., A. Levi, and J. Bridge. 1994. Relation between reverse sodium–calcium exchange and sarcoplasmic reticulum calcium release in guinea pig ventricular cells. *Circ. Res.* 74:550–554.

Leblanc, N., and J. Hume. 1990. Sodium current-induced release of calcium from cardiac sarcoplasmic reticulum. *Science.* 248:372–376.

Levesque, P., N. Leblanc, and J. Hume. 1994. Release of calcium from guinea pig cardiac sarcoplasmic reticulum induced by sodium–calcium exchange. *Cardiovasc. Res.* 28:370–378.

Levi, A. 1991. The effect of strophanthidin on action potential, calcium current and contraction in isolated guinea-pig ventricular myocytes. *J. Physiol.* 443:1–23.

Levi, A. 1993. A role for sodium/calcium exchange in the action potential shortening caused by strophanthidin in guinea pig ventricular myocytes. *Cardiovasc. Res.* 27:471–481.

Levi, A., K. Spitzer, O. Kohmoto, and J. Bridge. 1994. Depolarization-induced Ca^{2+} entry via Na^+–Ca^{2+} exchange triggers SR release in guinea pig cardiac myocytes. *Am. J. Physiol. Heart Circ. Physiol.* 266:H1422–H1433.

Levi, A. J., G. R. Dalton, J. C. Hancox, J. S. Mitcheson, J. Issberner, J. A. Bates, S. J. Evans, F. C. Howarth, I. A. Hobai, and J. V. Jones. 1997. Role of intracellular sodium overload in the genesis of cardiac arrhythmias. *J. Cardiovasc. Electrophysiol.* 8:700–721.

Litwin, S., O. Kohmoto, A. Levi, K. Spitzer, and J. Bridge. 1996. Evidence that reverse Na^+–Ca^{2+} exchange can trigger SR calcium release. *Ann. NY Acad. Sciences.* 779:451–463.

Litwin, S., J. Li, and J. Bridge. 1998. Na^+–Ca^{2+} exchange and the trigger for sarcoplasmic reticulum Ca^{2+} release: studies in adult rabbit ventricular myocytes. *Biophys. J.* 75:359–371.

Litwin, S. E., and J. H. B. Bridge. 1997. Enhanced Na^+–Ca^{2+} exchange in the infarcted heart. *Circ. Res.* 81:1083–1093.

Lu, H., and F. de Clerck. 1993. R56865, a Na^+/Ca^{2+}-overload inhibitor, protects against aconitine-induced cardiac arrhythmias in vivo. *J. Cardiovasc. Pharmacol.* 22:120–125.

Luk, H. N., and E. Carmeliet. 1990. Na^+-activated K^+ current in cardiac cells: rectification, open probability, block and role in digitalis toxicity. *Pflug. Archiv. Eur. J. Physiol.* 416:766–768.

Luo, C. H., and Y. Rudy. 1994a. A dynamic model of the cardiac ventricular action potential. I. Simulations of ionic currents and concentration changes. *Circ. Res.* 74:1071–1096.

Luo, C. H., and Y. Rudy. 1994b. A dynamic model of the cardiac ventricular action potential. II. Afterdepolarizations, triggered activity, and potentiation. *Circ. Res.* 74:1097–1113.

Matsuoka, S., and D. Hilgemann. 1992. Steady-state and dynamic properties of cardiac sodium–calcium exchange. Ion and voltage dependencies of the transport cycle. *J. Gen. Physiol.* 100:963–1001.

Nagatomo, T., Z. Fan, B. Ye, G. Tonkovich, C. January, J. Kyle, and J. Makielski. 1998. Temperature dependence of early and late currents in human cardiac wild-type and long Q-T ΔKPQ Na^+ channels. *Am. J. Physiol. Heat Circ. Physiol.* 275:H2016–H2024.

Nakao, M., and D. Gadsby. 1989. [Na] and [K] dependence of the Na/K pump current–voltage relationship in guinea pig ventricular myocytes. *J. Gen. Physiol.* 94:539–565.

Nuss, H., and S. Houser. 1992. Sodium–calcium exchange-mediated contractions in feline ventricular myocytes. *Am. J. Physiol. Heart Circ. Physiol.* 263:H1161–H1169.

Radford, N. B., J. D. Makos, R. Ramasamy, A. D. Sherry, and C. R. Malloy. 1998. Dissociation of intracellular sodium from contractile state in guinea-pig hearts treated with ouabain. *J. Mol. Cell. Cardiol.* 30: 639–647.

Ravens, U., and H. Himmel. 1999. Drugs preventing Na^+ and Ca^{2+} overload. *Pharmacol. Res.* 39:167–174.

Sanguinetti, M. C. 1990. Na^+-activated and ATP-sensitive K^+ channels in the heart. *In* Potassium Channels: Basic Function and Therapeutic Aspects. T. J. Colatsky, editor. Alan R. Liss, Inc, New York. 85–109.

Shaw, R., and Y. Rudy. 1997. Electrophysiologic effects of acute myocardial ischemia: a theoretical study of altered cell excitability and action potential duration. *Cardiovasc. Res.* 35:256–272.

Sipido, K., M. Maes, and F. van de Werf. 1997. Low efficiency of Ca^{2+} entry through the Na^+–Ca^{2+} exchanger as trigger for Ca^{2+} release from the sarcoplasmic reticulum. A comparison between L-type Ca^{2+} current and reverse-mode Na^+–Ca^{2+} exchange. *Circ. Res.* 81:1034–1044.

Smith, T., E. Antman, P. Friedman, C. Blatt, and J. Marsh. 1984. Digitalis glycosides: mechanisms and manifestations of toxicity. *Prog. Cardiovasc. Dis.* 26:413–458, 495–523; 27:21–56.

Tani, M., and J. Neely. 1990. Na^+ accumulation increases Ca^{2+} overload and impairs function in anoxic rat heart. *J. Mol. Cell. Cardiol.* 22:57–72.

van Echteld, C., J. Kirkels, M. Eijgelshoven, P. van der Meer, and T. Ruigrok. 1991. Intracellular sodium during ischemia and calcium-free perfusion: a ^{23}Na NMR study. *J. Mol. Cell. Cardiol.* 23:297–307.

Varghese, A., and G. Sell. 1997. A conservation principle and its effect on the formulation of Na^+–Ca^{2+} exchanger current in cardiac cells. *J. Theoret. Biol.* 189:33–40.

Veldkamp, M. W., J. Vereecke, and E. Carmeliet. 1994. Effects of intracellular sodium and hydrogen ion on the sodium activated potassium channel in isolated patches from guinea pig ventricular myocytes. *Cardiovasc. Res.* 28:1036–1041.

Viswanathan, P., R. Shaw, and Y. Rudy. 1999. Effects of I_{Kr} and I_{Ks} heterogeneity on action potential duration and its rate dependence: a simulation study. *Circulation.* 99:2466–2474.

Vornanen, M., N. Shepherd, and G. Isenberg. 1994. Tension–voltage relations of single myocytes reflect Ca release triggered by Na/Ca exchange at 35 degrees C but not 23 degrees C. *Am. J. Physiol. Cell Physiol.* 267:C623–C632.

Wang, D. Y., S. W. Chae, Q. Y. Gong, and C. O. Lee. 1988. Role of a^i_{Na} in positive force-frequency staircase in guinea pig papillary muscle. *Am. J. Physiol. Cell Physiol.* 255:C798–C807.

Wang, Z., T. Kimitsuki, and A. Noma. 1991. Conductance properties of the Na^+-activated K^+ channel in guinea-pig ventricular cells. *J. Physiol.* 433:241–257.

Wasserstrom, J., and A. Vites. 1999. Activation of contraction in cat ventricular myocytes: effects of low Cd^{2+} concentration and temperature. *Am. J. Physiol. Heart Circ. Physiol.* 277:H488–H498.

Wendt-Gallitelli, M. F., T. Voigt, and G. Isenberg. 1993. Microheterogeneity of subsarcolemmal sodium gradients. Electron probe microanalysis in guinea-pig ventricular myocytes. *J. Physiol.* 472:33–44.

Wier, W., and P. Hess. 1984. Excitation–contraction coupling in cardiac Purkinje fibers. Effects of cardiotonic steroids on the intracellular [Ca^{2+}] transient, membrane potential, and contraction. *J. Gen. Physiol.* 83: 395–415.

Zeng, J., K. R. Laurita, D. S. Rosenbaum, and Y. Rudy. 1995. Two components of the delayed rectifier K^+ current in ventricular myocytes of the guinea pig type. Theoretical formulation and their role in repolarization. *Circ. Res.* 77:140–152.

Zeng, J., and Y. Rudy. 1995. Early afterdepolarizations in cardiac myocytes: mechanism and rate dependence. *Biophys. J.* 68:949–964.